Geothermics 66 (2017) 40–47

Contents lists available at ScienceDirect

Geothermics

journal homepage: www.elsevier.com/locate/geothermics

Use of tracers and temperature to estimate fracture surface area for EGS reservoirs

G. Michael Shook[a,*], Anna Suzuki[b]

[a] Mike Shook & Associates
[b] Stanford University, United States

ARTICLE INFO

Article history:
Received 7 November 2016
Received in revised form
12 December 2016
Accepted 15 December 2016

ABSTRACT

A key uncertainty in the design and long-time behavior of EGS reservoirs, and their management, is the fracture surface area that controls the rate of heat transfer between the host rock and the circulating injected water. A workflow is developed that uses analytic solutions to estimate this surface area. We first analyze a tracer test to estimate the fracture pore volume swept, the flow geometry, and the presence of multiple fractures (or damage zones around the primary fracture). Using this information about fracture properties, an analytic solution describing produced temperature vs. time can be solving iteratively to estimate surface area. In the case of multiple fractures, we show that the equation governing the produced fluids' temperature is superposed to estimate the surface area. The workflow is shown to be robust, even in the presence of heterogeneity.

The workflow is then used to make design decisions and predictions about the sustainably of a reservoir. Also shown is the use of the workflow to estimate power generation as a function of fracture properties (measured) and flow rates (controlled), and show how to scale up to multiple production wells and fracture packs. Assumptions used, and limitations of the method are discussed.

1. Introduction

Engineered Geothermal Systems (EGS) rely on the injection of cold water into one or more fractures in hot, low permeability host rock to "mine" the heat from the rock and produce hot water in one or more production wells. A key uncertainty is the fracture surface area that controls the rate of heat transfer between the host rock and the circulating injected water (Carslaw and Jaeger, 1959; Gringarten et al., 1975; Gringarten and Sauty, 1975); the method also relies on thermal properties of the rock and water (heat capacity, thermal diffusivity, etc.) but these properties can be measured or estimated easily. If estimated, the work by Stopa and Wojnarowski (2004) shows that the use of constant thermal properties introduced approximately 10% errors compared to analytic solutions.

Carslaw and Jaeger (1959) show analytic solutions for heat exchangers with 1-D flow in the "fracture" and no flow in the "matrix." Robinson and Tester (1984) and Robinson et al. (1988) used similar equations in matching production temperature histories for two EGS projects by adjusting the surface area of the fracture, but note the problem in using tracers to determine the distribution of fractures in space. Shan and Pruess (2005) use a 2-D geometry with uniform flow per fracture to show the specific surface area (A/V_B) can be estimated using a diffusing tracer. Pruess and Doughty (2010) show that matching huff-n-puff tests using temperature as a tracer is useful to estimate changes in heat transfer area but show no explicit calculation for surface area. Dean et al. (2015) showed the use of cation exchange and numerical simulation to estimate fracture surface area, but the method relies on the accuracy of the reservoir properties used in the simulation.

Robinson and Tester (1984) also showed a relationship between heat exchange surface area and reservoir volume for two EGS reservoirs. This correlation demonstrates the need to estimate both fracture volume and surface area to optimize EGS heat extraction over reservoir life. The purpose of this work is to develop a method to simultaneously estimate fracture pore volume, flow geometry, and fracture surface area using conservative tracers and temperature in analytic solutions.

* *Corresponding author.
E-mail address: mike@mikeshookassoc.com (G.M. Shook).

http://dx.doi.org/10.1016/j.geothermics.2016.12.006
0375-6505/

Nomenclature

A	Surface area [m^2]
A_i	Surface area of the "i" fracture [m^2]
b	Half aperture of the fracture [m]
C	Concentration of tracer [kg/m^3]
C_p	Heat capacity [J/kg/K]
F	Cumulative flow capacity of the fracture set
f	Flow capacity of the "i" fracture [m^3/s]
k_{fract}	Permeability of the fracture [m^2]
K_R	Thermal conductivity of the rock [J/s/m/K]
L	Minimum spacing between "fracture packs" [m]
M_K	Mass of tracer injected [kg]
m_p	Mass of tracer produced [kg]
$\dot{m}_j$	The mass flow rate in the jth production well
OF	Objective function
q_J	Volumetric rate [m^3/s]
q	Volumetric injection rate [m^3/s]
q_i	Volumetric rate of the "i" fracture [m^3/s]
q_P	Volumetric production rate [m^3/s]
S	Surface area of the fracture [m^2]
t	Time [s]
t^*	Tracer mean residence time [s]
T_{amb}	Reinjection (or ambient) temperature [°C]
T_D	Dimensionless temperature [–]
T_F	Field temperature [°C]
T_i	Temperature of the "i" fracture [°C]
T_I	Initial temperature [°C]
T_J	Injected temperature [°C]
T_M	Model temperature [°C]
T_{Mi}	Model temperature of the "i" fracture [°C]
T_R	Temperature in the rock matrix [°C]
t_{Slug}	Time over which tracer is injected [s]
T_w	Temperature in the fracture [°C]
V_p	Pore volume [m^3]
V_{pi}	Pore volume of the "i" fracture [m^3]
V_s	Total pore volume swept [m^3]
W	Fracture width [m]
z	Axis perpendicular to the fracture [m]
Greek	
η	Thermal to electric power conversion efficiency
ρ_i	Density (i = water w, but rock, R) [kg/m^3]
τ	Residence time of a flowpath [s]
ϕ	Porosity [–]
ϕ_{fract}	Porosity of the fracture [–]
Φ	Cumulative storage capacity of the fracture set
φ_i	The storage capacity of the "i" fracture [m^3]

2. Proposed method

2.1. Estimating temperature

The governing equations in Gringarten and Sauty (1975), which are similar to that by Lauwerier (1955) and Carslaw and Jaeger (1959), can be written for flow in a fracture with conduction of heat in the surrounding rock

$$\frac{b}{2}\left(\rho C_p\right)_T \frac{\partial T_w}{\partial t} + \frac{q}{2}\left(\rho C_p\right)_w \frac{\partial T_w}{\partial S} - K_R \frac{\partial T_R}{\partial z}\Big|_{z=b/2} = 0 \tag{1}$$

for the fracture (see Nomenclature for a definition of variables) with $(\rho C_p)_T = \phi(\rho C_p)_w + (1-\phi)(\rho C_p)_R$. The surrounding rock matrix temperature is governed by the following equation.

$$\frac{(\rho C_p)_R}{K_R}\frac{\partial T_R}{\partial t} - \frac{\partial^2 T_R}{\partial z^2} = 0 \tag{2}$$

The temperatures also satisfy the following initial and boundary conditions.

$$T_w(S,t) = T_R(S,z,t) = T_I \quad t \le \frac{\phi b S}{q} \tag{3a}$$

$$T_w(0,t) = T_J \quad t > 0 \tag{3b}$$

$$T_w(S,t) = T_R(S,b/2,t) \quad \forall S,t \tag{3c}$$

$$lim_{z\to\infty} T_R(S,z,t) = T_I \quad \forall S,z,t \tag{3d}$$

Gringarten and Sauty (1975) show the solution of Eqs. (1) and (2), subject to constraints Eq. (3), is

$$\frac{T_I - T_w(t)}{T_I - T_J} = erfc\left[\frac{(\rho C_p)_w^2}{K_R(\rho C_p)_R}\left(\frac{q}{S}\right)^2\left\{t - \frac{\left(\rho C_p\right)_T}{\left(\rho C_p\right)_w}\frac{bS}{q}\right\}\right]^{-1/2} \tag{4}$$

We use the following identities to write Eq. (4) in terms the surface area of the fracture and other variables more easily measured or controlled.

$$V_p = bWL\varphi = bS\varphi \tag{5}$$

$$A = 2S \tag{6}$$

And multiplying the last term in Eq. (4) by ϕ/ϕ and simplifying, we get

$$T_w(L,t) = T_I - (T_I - T_J)erfc\left[\frac{1}{(\rho C_p)_w}\frac{A}{2q}\sqrt{K_R(\rho C_p)_R}\frac{1}{\left(t - \frac{(\rho C_p)_T}{(\rho C_p)_w}\frac{V_p}{\varphi q}\right)^{1/2}}\right] \tag{7}$$

The utility of Eq. (7) above consists of writing the equation in variables that can be measured (e.g., T, K_R, C_p, V_p – see below) or controlled (q) except the fracture surface area, A. Thus, by measuring the thermal properties of the rock and water as a function of temperature and measuring the produced temperature, we can solve Eq. (7) for surface area using a non-linear solver (in our case, we use Excel).

There is one more "unknowable" that shows up in Eq. (5), fracture porosity ϕ. Porosity is part of the total heat capacity term $(\rho C_p)_T$. But from a volumetric perspective, since $(1-\varphi)(\rho C_p)_R$ is the same magnitude as $\varphi(\rho C_p)_w$, any errors in ϕ are second order. The only other term containing ϕ is the time lag term but it also second order. We have used ϕ between 0.95 and 0.7 in the examples, without discernable differences.

2.2. Tracer testing to estimate pore volume and flow geometry

2.2.1. Total pore volume swept

Tracer interpretation methods have been developed in recent years to offer a wide range of reservoir and flood properties. In particular, the following properties can be determined from conservative tracers (Shook and Forsmann, 2005; Shook et al., 2009):

- Total pore volume swept, V_s:

It is the product of the tracer mean residence time, t^* and interwell flow rate, q.

- The flow geometry of the individual flow paths, f and φ:

That is, the fraction of the total flow rate associated with a given flow path, and the pore volume associated with that flow rate. This information is used to superpose an arbitrary number of 1-D solutions using Eq. (7) (see Example 2 below).

- The residence time distribution of the flow field, calculated as dF/dΦ

This information gives an idea of the number of "fractures" in the domain. A fracture is identified by a constancy of residence times by the number of flowpaths.

For a conservative tracer injected as a slug over time t_{slug}, the total volume swept for a given well pair, V_s, is determined from tracer concentration histories at the production well as follows:

$$V_S = q_J \frac{m_P}{M_\kappa}\left(\frac{\int_0^\infty q_p C t dt}{\int_0^\infty q_p C dt} - \frac{t_{Slug}}{2}\right) \tag{8}$$

where m_P is the tracer mass recovered in the production well, and M_K is the total mass of tracer "κ" injected, q_P is the production rate, and q_J is the injection rate. Thus, the first two terms in Eq. (8) represent the interwell volumetric flow rate, and the remainder of Eq. (8) is the mean residence time of the tracer. The use of the fraction of tracer produced in calculating interwell flow rate corrects for multiple production wells and leak-off. When the injection rate fluctuates, we have found it is best to use an average value in these equations.

Obviously, the upper limit of integration in Eq. (8) can pose difficulties in interwell tracer tests. Tracer tests are frequently terminated before the tracer response goes to zero because the tracer concentration decreases to values less than the detection limit, or the concentration data become too noisy for accurate calculations, or simply because the sampling is terminated for one reason or another. However, failure to account for the tracer tail will underestimate the swept pore volume. Tracer concentrations frequently decline exponentially, such that ln(Concentration) vs. time is linear. The means of using exponential decline is given in Shook and Forsmann (2005) and Shook et al. (2009). Other ways to extrapolate the tail of a tracer history are given in Shook et al. (2016). Extrapolating the tracer curve for this application is not expected to be needed, since the tracer is injected at the onset of injection, and injection is expected to last long after tracer concentration goes to zero. We are interested in the decline of the temperature history, which lags the tracer by a factor proportional to the ratio of heat capacities – usually a factor of 10 for EGS properties. The interested reader is directed to the literature for methods of extrapolating the curves.

2.2.2. Flow geometry and estimating fracture properties

Tracers can be used to estimate the flow geometry of the fractured media as first shown by Shook (2003) and Shook and Forsmann (2005). Flow capacity – storage capacity diagrams have appeared in petroleum reservoir engineering literature for decades (Stiles, 1949; Schmalz and Rahme, 1950; Lake, 1989; Gunter et al., 1997). Also known as F-C curves, they were originally derived for 2-D, vertical cross section, non-communicating, layered reservoirs. Shook and Forsmann (2005) and Shook et al. (2009) generalized F-C curves to use dynamic data e.g. tracers and termed the dynamic Flow capacity – Storage capacity curve (F-Φ curve). Briefly, the flow capacity of an arbitrary flowpath, f_i, is the volumetric rate of the flowpath divided by the total flow rate, and the storage capacity, φ_i, is the fraction of pore volume associated with the flowpath:

$$f_i = \frac{q_i}{\sum_{j=1}^{N} q_j} = \frac{q_i}{q_T} \tag{9}$$

$$\varphi_i = \frac{V_{Pi}}{\sum_{j=1}^{N} V_{Pj}} = \frac{V_{Pi}}{V_S} \tag{10}$$

The F-Φ curve is simply a cumulative curve of the individual flowpaths' f and φ. Shook (2003) and Shook and Forsmann (2005) show the F-Φ curve can be estimated from tracer data as shown in Eqs. (11) and (12) below.

$$F(t) = \frac{\int_0^t qC d\tau}{\int_0^\infty qC dt} \tag{11}$$

$$\Phi(t) = \frac{\int_0^t qC\tau d\tau}{\int_0^\infty qCt dt} \tag{12}$$

F-Φ curves are used qualitatively and quantitatively, for example "60% of the flow is coming from 12% of the pore volume." We also show the F-Φ curve is useful in estimating the number of "fractures" in a reservoir (defined by the same residence time). This is the characteristic property of F-Φ curves that is valuable in the present context.

Wu et al. (2008) showed for a case of constant injection and production rates, the slope of the F- Φ curve is

$$\frac{dF}{d\Phi} = \frac{1}{t}\frac{\int_0^\infty Ct dt}{\int_0^\infty Cdt} = \frac{t^*}{\tau} \tag{13}$$

where τ is the residence time of a given streamline and t^* is the mean residence time. So the relative slope gives insight into the number of fractures (or, more generally, the presence of different permeabilities – in the case of one fracture with damaged zones around it) seen by the tracer. We can estimate the fraction of the flow rate and pore volume associated with individual fractures by noting the breaks in the F-Φ curve slope. We use this property of F-Φ curves to superpose analytic temperature solutions in Example 2 below.

2.2.3. Workflow

The previous sections show that, by writing the solution for producer temperature vs. time in terms of variables that can be measured (including pore volume from tracer testing) or can be controlled (total injection rate), we can estimate the surface area that controls conduction in EGS reservoirs. In the case of damage zones around the fracture (a result of the stimulation job), we use the F-Φ curve to estimate the fraction of volumetric rate (Eq. (11))

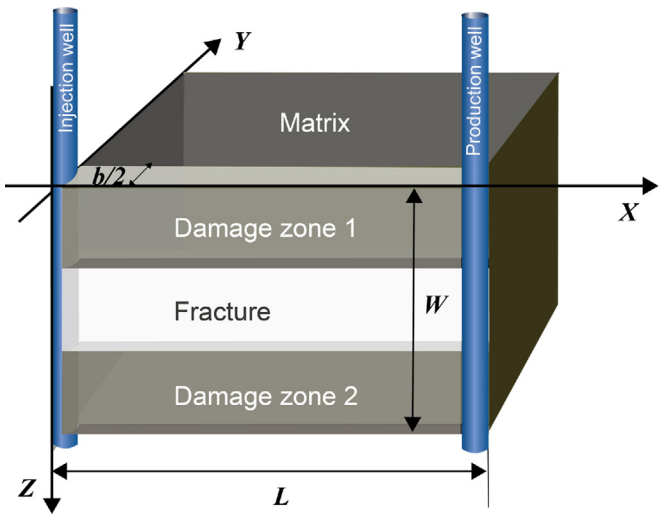

Fig. 1. A schematic of the EGS reservoir used in this study. Example 1 below assumes the fracture is uniform and encompasses the two "damage zones." Example 2 assumes the damage zones have different permeability and porosity, see Table 1.

and pore volume associated with these fractures (Eq. (12)). In this case, Eq. (7) written for all fractures (using the individual fractures' V_{pi} and q_i) and the results are summed. We show an example of this in Example 2 below.

Our workflow to estimate surface area in EGS reservoirs proceeds as follows. Given injection and production wells, both stimulated to insure good connectability:

1. Run a tracer test; estimate total pore volume swept using Eq. (8) and the flow geometry using Eqs. (11) and (12). Based on the number of abrupt breaks in the F-Φ curve slope estimate the number of "fractures" and the fraction of the total rate and fraction of the pore volume associated with each fracture. Convert these to the fractures' pore volume and rate.
2. Based on the number of fractures, write the production temperature as a sum of the solution of Eq. (7) for every fracture. If we denote the model temperature $T_M = T_{M1} + T_{M2} + \ldots T_{Mn}$, next we compare field temperatures T_F with T_M at every time field data is collected. We now define an Objective Function, $OF = \Sigma(T_F - T_M)^2$ where the errors are summed over time. We have N unknowns where N is the number of fractures. We next provide an initial estimate for the fracture surface area A_i and use a non-linear solver to minimize OF by changing the A_i.

In what follows, we restrict our calculations to a single well pair, but we consider first one fracture, and then one fracture with damage on either side, and show the benefits of using the workflow. We then show some examples of the use of such information, show scaleup to field scale (multiple well pairs and multiple fractures) and implications of the study results.

3. Verification

3.1. Model description

The model used for this study was a single well pair completed in a single vertical fracture set in non-fractured native rock. The half-length of the fracture is 99 m with a height of 75 m and an aperture of 0.02 m. The matrix width is 642.66 m to ensure semi-infinite media over the time scale of interest, with grid block sizes increasing by a factor of 2 away from the fracture to ensure numerical error is controlled. The wells are completed only in the fracture. See Fig. 1 for a schematic of the model. Thermal and physical properties of the rock were taken from the literature and are summarized in Table 1. The matrix is assumed to have no permeability and the fracture permeability depends on the example number.

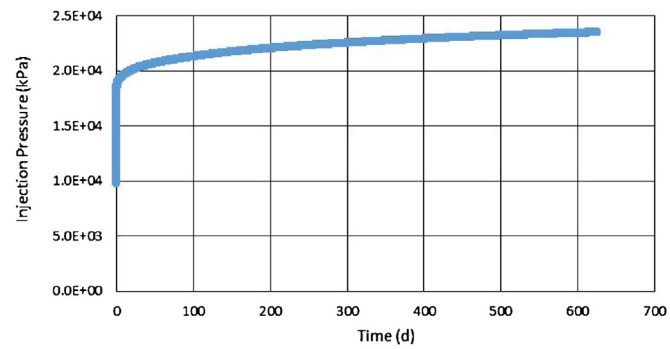

Fig. 2. Injection Pressure vs. time for Example 1 (base case).

The initial temperature is 200 °C, and the initial pressure is set to 9800 kPa, about the hydrostatic pressure gradient assuming the fracture is at 1 km depth. At $t = 0$, water at 25 °C is injected for 1 h, followed with 25 °C water with 10% tracer for one hour and then with 25 °C water without tracer for the balance of the simulation. All injection and production rates are 2 kg/s. For reasons of symmetry we simulated a half-space solution, but the results showed below are for the full solution for a single well pair with rock surrounding the fracture. The results are scaled up to field scale in a following section (multiple production wells, and multiple fracture packs, etc.).

For the examples showed here, we use TOUGH2 (Pruess, 1991) to simulate the "true" reservoir and displacement properties (including pore volume swept, surface area, and temperature histories), and then calculate the pore volume swept using the tracer and the temperature history to estimate the fracture surface area. An acceptable comparison of surface area validates the method and gives us confidence in predicting the performance of the EGS reservoir. Of course, these predictions are only valid for the specific reservoir properties we used in our study; the calculations would need to the performed anew for a specific EGS field test. The main objective of the paper is to introduce the workflow needed to make these predictions.

3.2. Example 1: single fracture

For our first case, we assume the fracture permeability is a constant 1.0×10^{-11} m^2 (~10 D) and an injection rate of 2 kg/s. Tracer is injected for one hour at a concentration of 10% by weight. After injecting tracer, injection is switched to chase fluids (water without tracer) for the duration of the field test. One of our concerns in starting these simulations was to choose an injection rate sufficiently low such that injection pressure stays below the parting pressure. We use a rate of 2 kg/s for the complete field test; the injection pressure history is given in Fig. 2. As can be seen, the injection pressure grows to 23,500 kPa or about lithostatic pressure at 620 days, suggesting our flow rates may be little high. This is an issue for field experiments, but it is acceptable for our purposes here.

The tracer test is only done to estimate the fracture pore volume, so we first analyze the tracer data. The tracer history is shown in Fig. 3 below. From Eq. (8), we can calculate the swept volume as 130.76 m^3. From Table 1, the true pore volume is 133.65 m^3 giving an error of 2.2%. We then can use the pore volume in Eq. (7) to estimate fracture surface area.

From Fig. 4, we can see the method presented can match the field temperatures well. Table 2 shows the estimated surface area, maximum error, and the objective function for the three times at

Table 1
A summary of EGS field properties used, including calculated values of fracture pore volume and surface area to verify the accuracy of the method.

Thermal Properties		Petrophysical Properties			
ρ_R (kg/m^3)	2569			Example 1	Example 2
Cp_R (J/kg C)	803			1 fracture	1 fracture between 2 damage zones
K_R (W/m C)	2.569	ϕfract			
ρ_w (25C) (kg/m3)	997.1		Damage zone 1	0.9	0.75
ρ_w(200C) (kg/m3)	864		Fracture		0.5
C_{pw} (25 °C) (J/kg K)	4180		Damage zone 2		0.95
C_{pw} (200 °C) (J/kg K)	4510	k_{fract} (10^{-12} m^2, ~D)			
Initial and Injection Conditions			Damage zone 1	10	4
Initial pressure@ 1 km, (kPa)	9800		Fracture		10
Initial temperature (°C)	200		Damage zone 2		2
Injection mass rate (kg/s)	2	"Truth"			
Injection temperature (°C)	25	Vp (m^3)			
Grid Properties			Damage zone 1	133.65	37.125
Model dimensions (m)	99 × 75 × 643		Fracture		24.75
Grid dimensions	33 × 15 × 3		Damage zone 2		47.025
DX (m)	3	Surface area (m^2)			
DY (m)	0.01, 0.02, 0.04, . . .		Damage zone 1	14,850	4950
DZ (m)	25		Fracture		4950
			Damage zone 2		4950

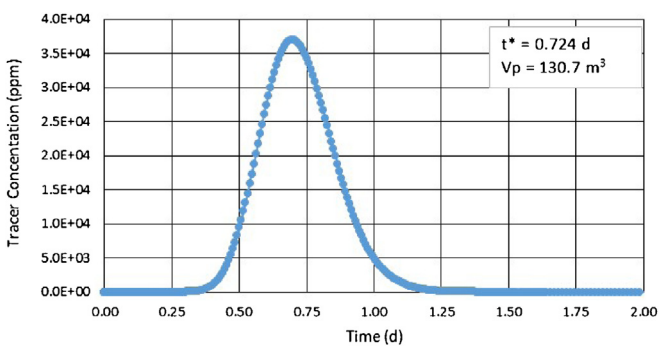

Fig. 3. Tracer history (tracer concentration vs. time) for Example 1.

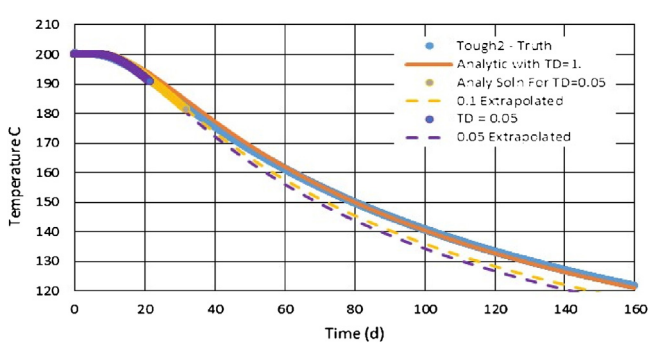

Fig. 4. "True" and Estimated Temperature Histories for Example 1. The start of the dotted line portion of the curves denotes the time at which the estimate of surface area is done for two extrapolation times.

Table 2
A summary of estimations of surface area and error for three termination temperature, compared with the value from the simulation inputs for Example 1.

	Termination temperature		
	$T_D = 1.0$	$T_D = 0.1$	$T_D = 0.05$
Estimated surface area (m^2)	14492.8	13727.5	13442.3
Objective Function	3903.8	242.1	72.9
Max error	3.86	0.55	0.33
Relative error	0.0241	0.0756	0.0948
True surface area (m^2)	14,850		

which the field test could be terminated. The first analytic curve assumes the field test was not terminated until the produced temperature falls to close to the injected temperature. We define the dimensionless temperature as:

$$T_D = \frac{T(t) - T_I}{T_J - T_I} \tag{14}$$

where T_I is the initial temperature and T_J is the injected. So, $T_D = 1$ is the full dataset, $T_D = 0.1$ is a 10% change in temperature, and 0.05 is a 5% change. The change in the curves from markers to dashed line represents the final time at which the field data is used in the estimate. Depending on the relative importance of time spent vs. accuracy the relative error is bounded by 0.025–0.095. The maximum error in Table 2 is maximum difference between the field data and the estimates, using an arbitrary final temperature change of 10 °C. Of course, the only time the full dataset is useful is if the injection rate is far larger than the reservoir can generate sustainable electricity from. This method can be used for a field test at rates such that the test is done before much heat is mined but still collects the data needed to calculate sustainable rates for the design requirements. We believe the value of this workflow is to conduct a field experiment at rates just below parting pressure as long as feasible to collect information to design a long-term EGS project.

3.3. Example 2: 1 fracture with 2 damage zones

Our first simulation assumes the stimulation job is perfect – the full fracture is one permeability with no damage zones. In Example 2 we acknowledge the possibility of a (smaller) fracture with damage zones on either side. This scenario uses the F-Φ curve to divide the pore volume swept and the injection rate between the three zones and superposition of the temperature solutions to arrive at the estimate of surface area.

Everything except the fracture permeability and porosity is the same as in Example 1 (see Table 1), including the tracer injection time and concentration. So we start with the tracer interpretation as usual, but we need the F-Φ curve here (we calculating the F-Φ curve for Example 1, but as expected it showed no effects of multiple flow paths). The tracer history for Example 2 is plotted in Fig. 5 and the resulting F-Φ curve in Fig. 6.

As we saw in the Example 1 tracer test, the results agree well with the true pore volume given in Table 1 (the relative error = 2.66%). The presence of multiple permeability flow paths does nothing to invalidate the use of tracer analyses to estimate pore volume swept, and in fact, the presence of three flow paths is evident in the history. Allocating flow and pore volume between the flow paths is most easily done with the F-Φ curve as shown in

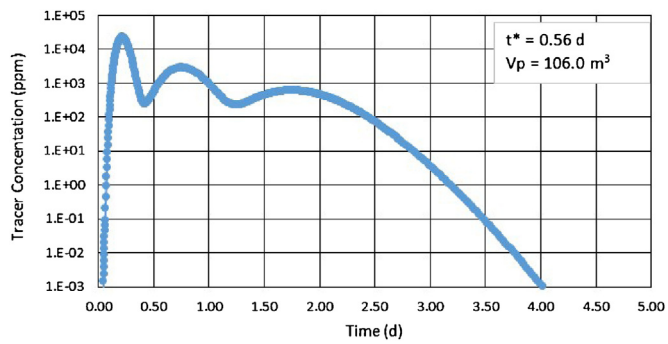

Fig. 5. The tracer history for Example 2. Notice the presence of the three fracture zones.

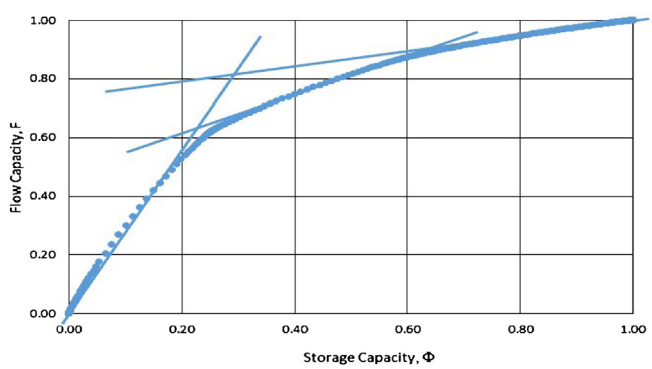

Fig. 6. The F-Φ for Example 2, showing the flow geometry and the apportioned rates and pore volumes between the three flow paths.

Table 3
Rates and Pore Volumes for the three flow paths from Fig. 6.

Zone	Φ_i (fraction of V_{pi})	F_i (fraction of q_i)	V_{pi} (m^3)	q_i (m^3/s)
Fracture	0.234	0.598	24.8	1.20
Damage zone 1	0.4	0.291	42.4	0.58
Damage zone 2	0.366	0.111	38.8	0.22

Fig. 6. This can also be done by plotting the derivative – dF/dΦ vs. Φ, as shown in Nalla and Shook (2005).

As mentioned previously, constancy in the slope of the F-Φ curve denotes the presence of a flow path (or a number of paths) with a single residence time (we have taken the liberty to also draw tangents to illustrate). Because we set the injection rate and we know the total pore volume from Fig. 5 above, we can use the F-Φ curve to apportion these properties between the flow paths, as shown in Table 3 below.

We then use the individual fracture properties to estimate the total surface area. Owing to the form of Eq. (7), we can use superposition for our three flow paths (using q and V_p from Table 3 for each path) and sum up the temperature histories:

$$T_M = (q_{fr}T_{fr} + q_{D1}T_{D1} + q_{D2}T_{D2})/q_P \tag{15}$$

where the subscripts denote the fracture and damage zones. The temperature history for Example 2 is shown in Fig. 7, and the estimations of surface area and errors using cutoff analysis times are given in Table 4. The accuracy of this method in the presence of heterogeneity is outstanding. Note we have used more of the data in the extrapolation due to the obvious variable residence times observed in Fig. 5, compared to Example 1.

For confirmation of the need for more data in the presence of heterogeneity, we also show the extrapolated temperature history calculated using only a 25% change in produced temperature in Fig. 7. Failure to conduct the field experiment long enough to see

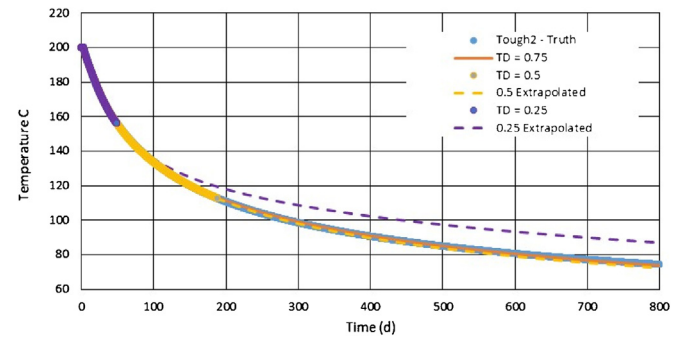

Fig. 7. The temperature history for Example 2 with three analytic estimates for Example 2 with extrapolation. Also shown is the ramifications of terminating the experiment early.

Table 4
A summary of estimations of surface area and error for three termination temperature, compared with the value from the simulation inputs for Example 2.

	Termination temperature		
	$T_D = 1.0$	$T_D = 0.75$	$T_D = 0.5$
Estimated surface area (m^2)	15623.4	15295.7	15269.1
Objective function	114224.9	42981.3	300.3
Max error	35.36	18.53	0.99
Relative error	−0.0521	−0.0300	−0.0282
True surface area (m^2)	14850		

the contributions of all fractures over-predicts late time temperatures. This also shows the value of our methodology in using a sufficiently large rate in the experiment to get the information in a timely fashion. This information is then used to design the EGS operations. We next show various uses of the workflow and scale up to field conditions.

4. Uses of the workflow

4.1. Optimization uses

Having conducted our "field experiment" to estimate surface area of the EGS reservoir, we are now able to use the workflow to answer questions about the design of an EGS project. We restrict these questions to our single well pair here, and scale up to more realistic field scale in the next section. The questions are also restricted to variables we have control over – injected temperature or injection rate. Any changes to the reservoir or injected fluid properties would need another tracer test, followed by injection of chase fluids to estimate the new surface area or pore volume.

For this example of using the workflow, we use the estimated reservoir properties from Tables 3 and 4 above and maximize the injection rate subjected to some field constraint. One question of interest might be: what maximum rate can we inject for no more than a 10% drop in producer temperature over 2 years? How about over 1 year? These two results are shown in Fig. 8 below. We also show the "true" temperature histories from running Tough2 on Example 2 reservoir properties but using the rates that give no more than 10% drop in temperature at the time of interest (1 or 2 years, for this example).

We can use the workflow to answer more relevant questions about the EGS operations but we need to scale up to field scale first. These questions will be illustrated in the following section.

4.2. Scale-up and implications for EGS

The examples above used a single well pair to show the utility of the workflow, but it seems obvious that the simplest well configura-

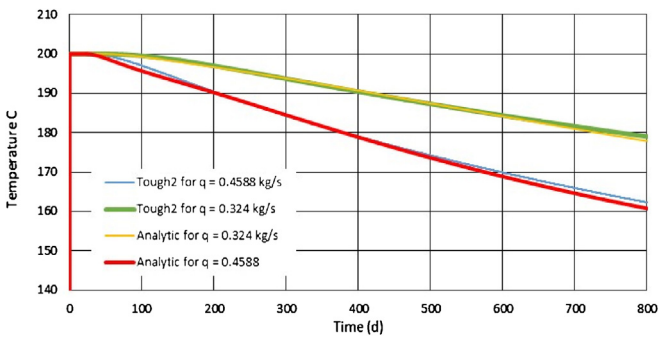

Fig. 8. Temperature histories for two prediction runs vs. "truth" for two optimized injection rates.

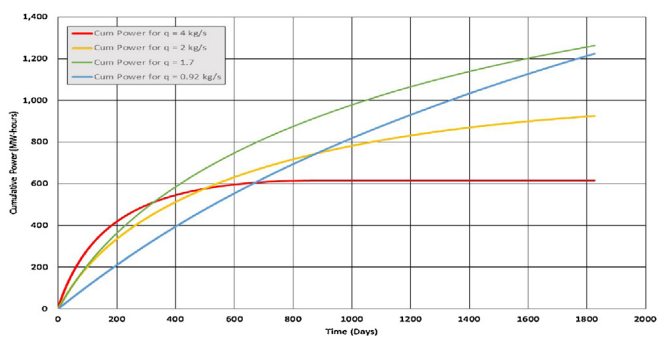

Fig. 9. A comparison in Cumulative Power Generated for 3 injection rates, 1 fracture but 2 wells.

tion in the field is one injection well between two production wells, with all wells having been stimulated to ensure good connectivity between injection and production. For this case, the tracer analysis is done in both well pairs and the workflow proceeds for each well pair.

For the purposes of this example, we assume the fracture properties are the same on either side of the injector. Thermal power produced is the sum of the two well pairs' production:

$$E(t) = \dot{m}_1 Cp_w (T_1 - T_{Amb}) + \dot{m}_2 Cp_w (T_2 - T_{Amb}) \tag{16}$$

where 1 and 2 refer to the producers (for our example, the rates and temperature histories are the same, otherwise the rates and the temperature histories come from the use of this workflow on the two well pairs) and T_{Amb} is the rejection (or ambient) temperature. Electric power is the product of thermal power and efficiency, η, We use the following equation for efficiency (Moon and Zarrouk, 2012):

$$\eta = 6.9681\ ln(T) - 29.713 \tag{17}$$

Eq. (17) is based on binary plants installed between 1984 and 2008, and so represents an average efficiency, implicitly averaging working fluid properties, turbine and generator efficiencies, inlet temperature, and vintage, for some examples of variables that influence efficiency. If the rejection temperature is 40 °C, we can deduce the electric capacity of the EGS reservoir studied here. We use Example 2 properties (and surface area estimates), and then run the workflow for different injection rates (and therefore different temperature histories). Four such cumulative power histories are shown in Fig. 9 below.

These solutions raise an interesting point: the higher rate can generate more electricity at early time, but the produced temperature falls quicker and so is not sustainable. If cumulative electricity generated is the screening criterion, it is obvious there is a balance between rate and the time necessary for the working fluid to "mine" the reservoir heat. This workflow could be used to optimize the EGS operations.

Of course there is no reason to limit the EGS development to only one fracture and two well pairs. By having two or more "fracture packs" within each well, the power output can be increased without drilling more wells, and so at a smaller cost. If the fractures are placed at least far enough away from each other so the temperature fronts do not interfere, this workflow can be used easily. The tracers in every production well will detect the presence of multiple fractures, and the F-Φ plot is used to apportion the flow and pore volume fractions as above. But, if the fracture sets are too close together and the temperature fronts interact, the semi-infinite boundary condition above (Eq. (3a)) is violated and the solution is artificially optimistic. The minimum spacing is a function of rock properties and time, as shown below (Bird et al., 1960 p. 354).

$$L = 4\sqrt{\frac{K_r t}{(\rho C_P)_T}} \tag{18}$$

There are other ways to make EGS projects seem more palatable; for example, the use of supercritical CO_2 (Pruess, 2006) as the working fluid (and the attendant tax breaks) seems worthwhile to consider but is out of scope for this paper. The workflow could be used with the appropriate changes in working fluid properties.

5. Summary and conclusions

We have presented a workflow that uses analytic solutions to estimate surface area available for heat conduction to working fluid in EGS environments. The novel contribution of the work is to write the temperature equation in terms that are either easily measured or controlled, including the fracture pore volume and the flow geometry. By using tracer testing and the F-Φ plot, we can deduce the presence of multiple fractures (or damage zones around the primary fracture) and use that information to superpose solutions and estimate the total surface area for an EGS reservoir. We also show how to use the workflow to estimate power generation as a function of fracture properties (measured) and flow rates (controlled), and show how to scale up to multiple production wells and "fracture packs."

The two most important limitations of the method are as follows. Any multiple "fracture packs" need to be placed far enough away so the temperature fronts do not interfere. The other (and maybe the most important) is the field test has to be conducted at rates such that the test is done before much heat is mined but still collects the data needed to calculate sustainable rates for the design requirements.

The most important assumption used in this work is the absence of permeability in the matrix (i.e. no fluid leakoff); further work is needed to relax this assumption. We also think (but have not proven) the method could be used in "enhanced" EGS reservoirs; that is, EGS reservoirs located on the flanks for hydrothermal reservoirs. There may be pre-existing fractures that may allow for larger flow rates. By using the F-Φ curve to identify "batches" of fractures that can be lumped together in the workflow. This too needs work to be established.

Acknowledgements

The authors are pleased to thank Stefan Finsterle and Curt Oldenburg at Lawrence Berkeley Lab for their help with TOUGH2, and Kit Bloomfield for useful discussions about power generation.

References

Bird, R.B., Steward, W.E., Lightfoot, E.N., 1960. Transport Phenomena. John Wiley & Sons.

Carslaw, H.W., Jaeger, J.C., 1959. Conduction of Heat in Solids, 2nd ed. Clarendon Press, Oxford.

Dean, C., Reimus, P., Oates, J., Rose, P., Newell, D., Petty, S., 2015. Laboratory experiments to characterize cation-exchanging tracer behavior for fracture surface area estimation at Newberry Crater, OR. Geothermics 53, 213–224, http://dx.doi.org/10.1016/j.geothermics.2014.05.011.

Gringarten, A.C., Sauty, J.P., 1975. J. Geophys. Res. 80 (35), 4956–4962.

Gringarten, A.C., Witherspoon, P.A., Ohnishi, Y., 1975. Theory of heat extraction from fractured hot dry rock. J. Geophys. Resour. 80 (8), 1120–1124, http://dx.doi.org/10.1029/JB080i008p01120.

Gunter, G.W., Finneran, J.M., Hartmann, D.J., Miller, J.D., 1997. Early determination of reservoir florw units using an integrated petrophysical method. Soc. Petrol. Eng., http://dx.doi.org/10.2118/38679-MS.

Lake, L.W., 1989. Enhanced Oil Recovery. Prentice Hall.

Lauwerier, H.A., 1955. The transport of heat in an oil layer caused by the injection of hot fluid. Appl. Sci. Res. A 5 (2), 145–150.

Moon, H., Zarrouk, S.J., 2012. Efficiency of geothermal power plants: a worldwide review. New Zealand Geothermal Workshop 2012 Proceedings.

Nalla, G., Shook, G.M., 2005. Novel application of single-well tracer tests to evaluate hydraulic stimulation effectiveness. Geotherm. Resour. Counc. Trans. 29, 177–181.

Pruess, K., Doughty, C., 2010. Thermal single-well injection-withdrawal tracer tests for determining fracture-matrix heat transfer area. Proceedings of the Thirty-Fifth Workshop on Geothermal Reservoir Engineering.

Pruess, K., 1991. TOUGH2—A General Purpose Numerical Simulator for Multiphase Fluid and Heat Transfer. Lawrence Berkeley Laboratory report LBL-29400, Berkeley, CA, USA (102 pp).

Pruess, K., 2006. Enhanced geothermal systems (EGS) using CO2 as working fluid—a novel approach for generating renewable energy with simultaneous sequestration of carbon. Geothermics 35 (4), 351–367, http://dx.doi.org/10.1016/j.geothermics.2006.08.002.

Robinson, B.A., Tester, J.W., 1984. Dispersed fluid flow in fractured reservoirs: an analysis of tracer-determined residence time distributions. J. Geophys. Res. 89 (B12), 10374–10384, http://dx.doi.org/10.1029/jb089ib12p10374.

Robinson, B.A., Tester, J.W., Brown, L.F., 1988. Reservoir sizing using inert and chemically reacting tracers. Soc. Pet. Eng., http://dx.doi.org/10.2118/13147-pa.

Schmalz, J.P., Rahme, H.D., 1950. The variation of waterflood performance with variation in permeability profile. Prod. Mon. 15 (9), 9–12.

Shan, C., Pruess, K., 2005. An analytical solution for slug tracer tests in fractured reservoirs. Water Resour. Res. 41, W08502, http://dx.doi.org/10.1029/2005WR004081.

Shook, G.M., Forsmann, J.H., 2005. Tracer interpretation using temporal moments on a spreadsheet. INL Rep., 05–00400.

Shook, G.M., Pope, G.A., Asakawa, K., 2009. Determining reservoir properties and flood performance from tracer test analysis. Soc. Pet. Eng., http://dx.doi.org/10.2118/124614-ms.

Shook, G.M., Sharma, A., Pope, G.A., 2016. Early time analysis of tracers for use in EOR flood optimization. Soc. Pet. Eng., http://dx.doi.org/10.2118/169109-PA.

Shook, G.M., 2003. A simple, fast method of estimating fractured reservoir geometry from tracer tests. Geotherm. Resour. Counc. Trans. 27, 407–411.

Stiles, W.E., 1949. Use of permeability distribution in waterflood calculations. J. Petrol. Technol. 1.01, 9–13.

Stopa, J., Wojnarowski, P., 2004. Analytical model of cold water front movement into geothermal reservoir. Geothermics 35 (1), 59–69.

Wu, X., Pope, G.A., Shook, G.M., Srinivasan, S., 2008. Prediction of enthalpy production from fractured geothermal reservoirs using partitioning tracers. Int. J. Heat Mass Transfer 51, 1453–1466.